

Bewegungsdetektion und -quantifizierung mittels InSAR (Satelliten-, UAV- und Bodengestützt)

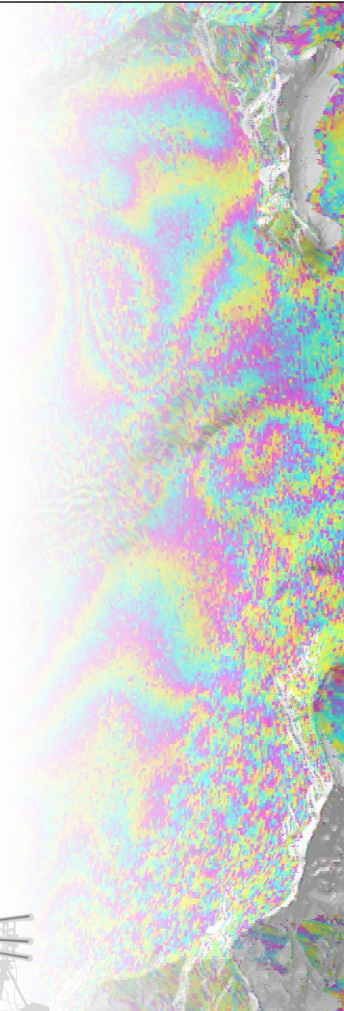
Stand der Entwicklung und Einsatzmöglichkeiten

Change detection and deformation monitoring using InSAR (spaceborne, UAV- and ground-based)

Current state of the art and field of application

Rafael Caduff & Urs Wegmüller

Gamma Remote Sensing AG, Gümligen, Switzerland - (caduff@gamma-rs.ch)

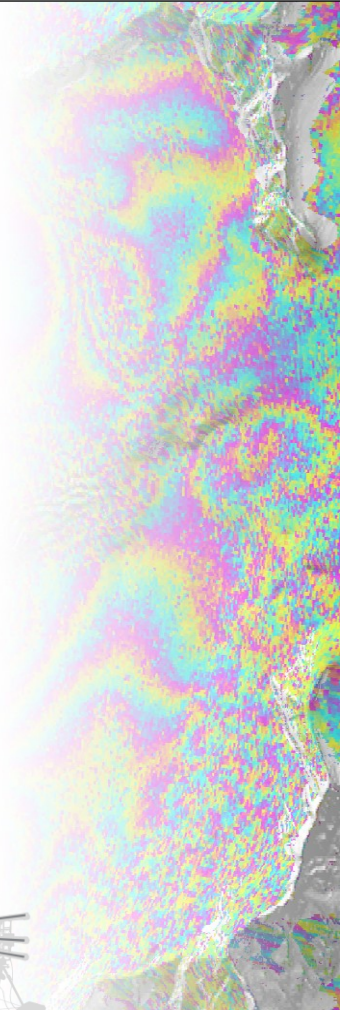




25 km

- Nature cover with the co-seismic ERS-1 satellite interferogram of the 1992 Landers earthquake (California)
- Shows the displacement field in Line of sight in color cycles for each phase cycle of 28 mm (C-Band) -> at least 560 mm shift in range
- **Start of an increasing width of applications in surface deformation monitoring**

Massonnet, D., Rossi, M., Carmona, C. et al. The displacement field of the Landers earthquake mapped by radar interferometry. Nature 364, 138–142 (1993). <https://doi.org/10.1038/364138a0>

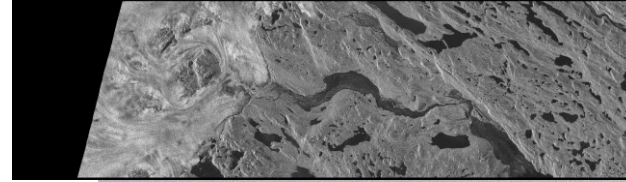




Active microwave sensor

Backscatter magnitude

T_0

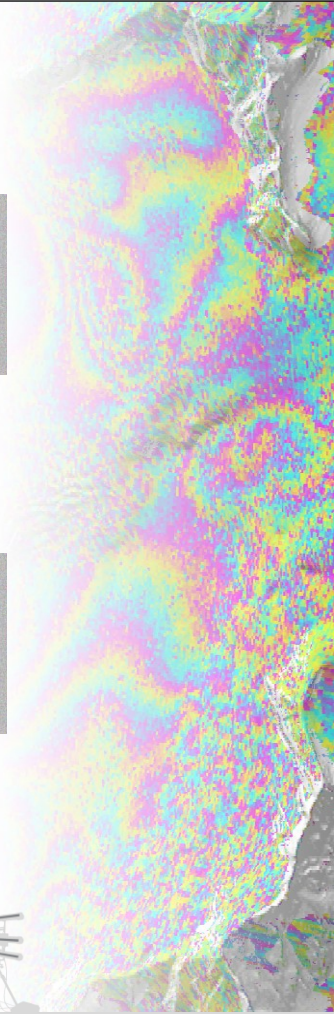


Coherent phase

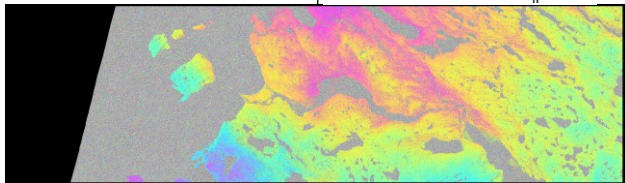
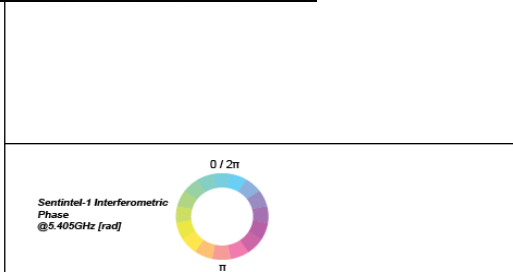
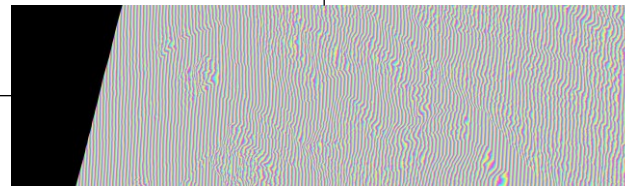
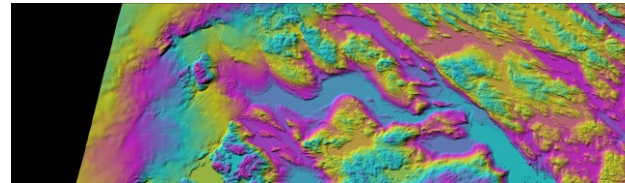
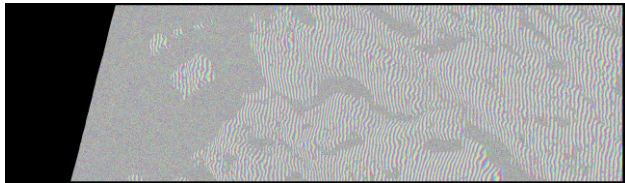
T_1



Complex valued SAR Image



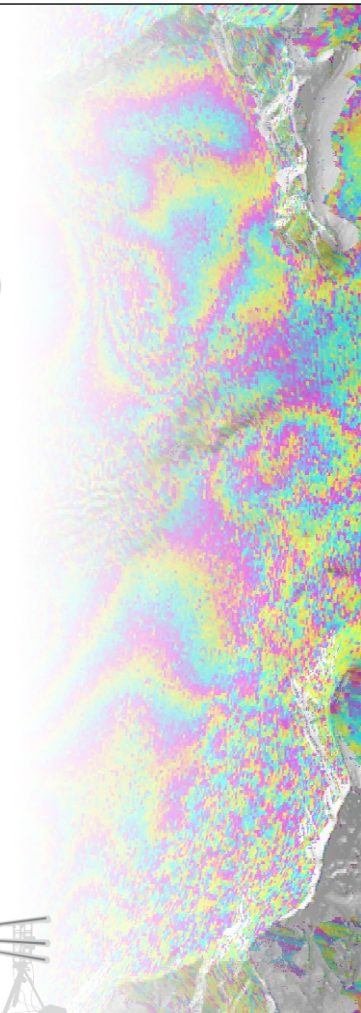
$$\varphi_{\text{int}} = \varphi_{\text{topo}} + \varphi_{\text{atmo}} + \varphi_{\text{disp}} + \varphi_{\text{noise}}$$



Differential Interferogram

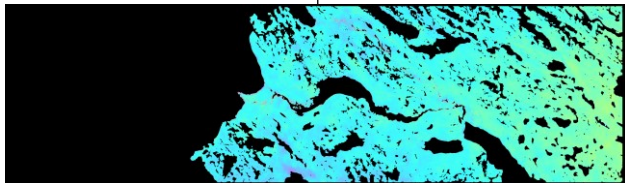
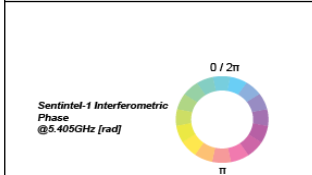
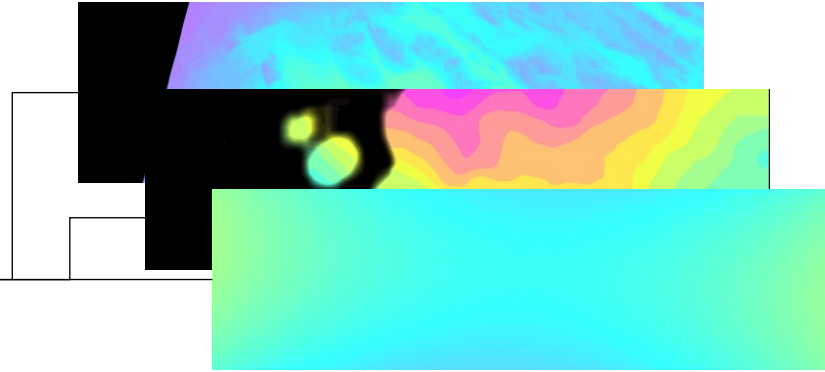
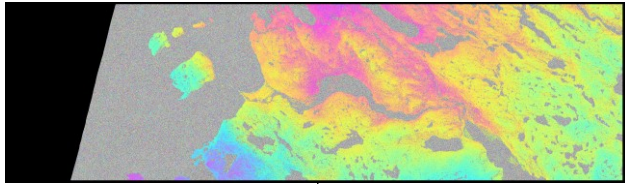
Simulated topographic phase (φ_{topo})

- Calculation based on digital elevation model (DEM) and perpendicular baseline (distance between the two satellite tracks) that is calculated from the satellite orbit state vectors.



$$\varphi_{\text{int}} = \varphi_{\text{topo}} + \varphi_{\text{atmo}} + \varphi_{\text{disp}} + \varphi_{\text{noise}}$$

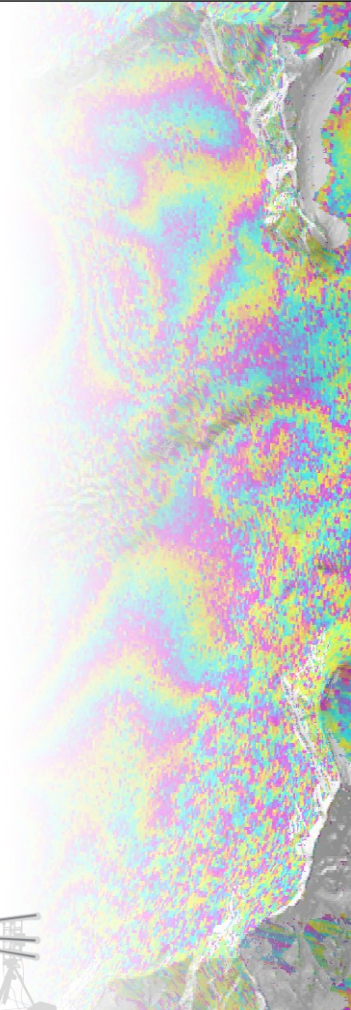
Sentinel-1 Interferometric Phase
@5.405GHz [rad]



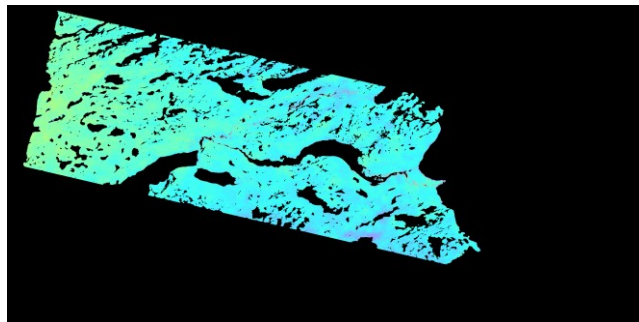
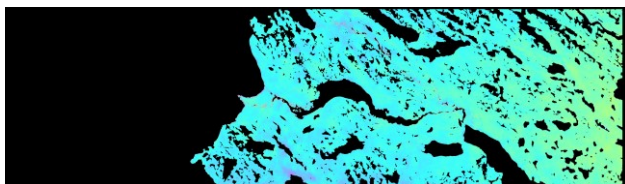
Filtered Differential Interferogram

Simulated atmospheric and ionospheric phase (φ_{atmo})

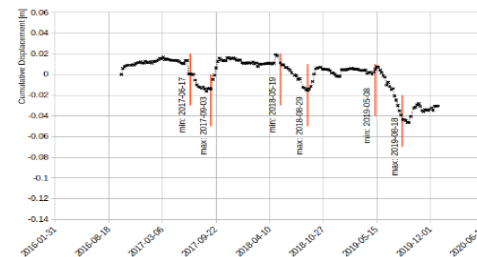
- Iterative calculation based on



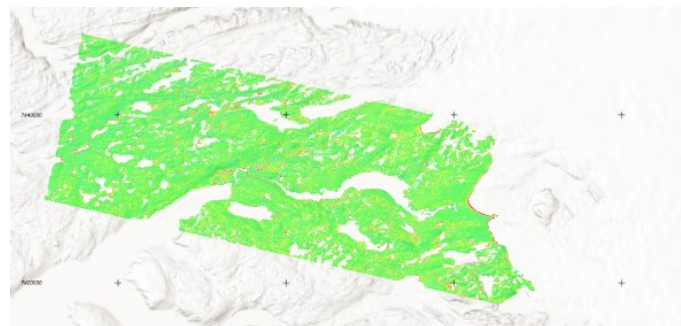
$$\varphi_{\text{int}} = \varphi_{\text{topo}} + \varphi_{\text{atmo}} + \varphi_{\text{disp}} + \varphi_{\text{noise}}$$



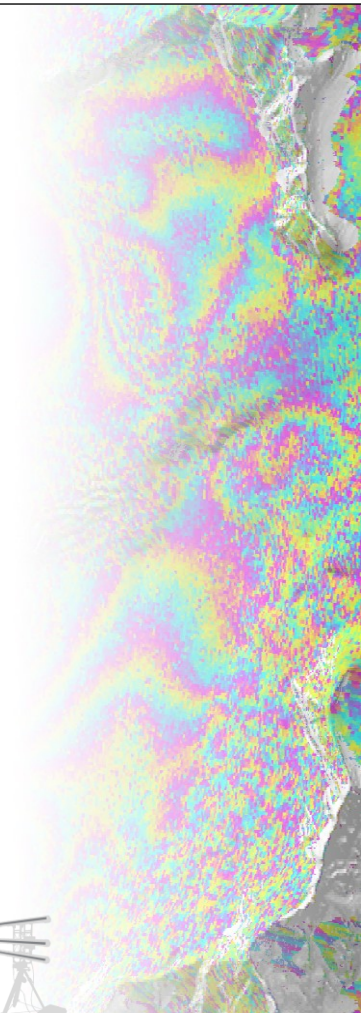
Geocoded filtered differential Interferogram



Point displacement time-series



Line-of-sight displacement map



Radar interferometry is **active sensing method** with which it is possible to detect and **quantify relative ground motion along the line of sight**.

- Precision

Depends on the used wavelength, the number of acquisitions, the ground cover properties and the kinematic of the motion.

A precision of **1 mm/yr** can be achieved (for X- and C-Band).

- Spatial ground resolution

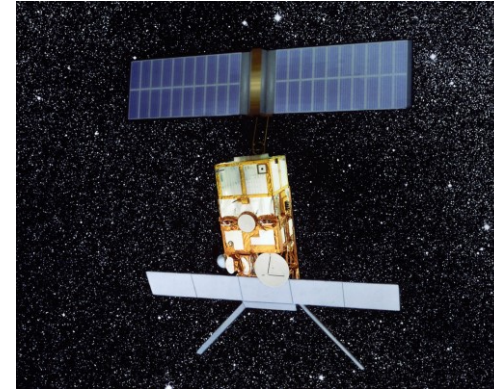
Highest resolutions of **50x50 cm** can be achieved (with staring-spotlight mode) with the downside of drastically reduced coverage. Sentinel-1 IW Mode for Global coverage has **20x5 m** nominal image resolution.

- Repeat intervals

Repeat intervals depend on the orbit. Interferometric applications need repeat paths that are as close together as possible. Repeat orbits of **35 days** were used for ERS, Sentinel-1 constellation of A and B has **6 day** repeat cycle. Commercial constellations can achieve programmed repeat intervals of **less than 1 day**.

- Costs

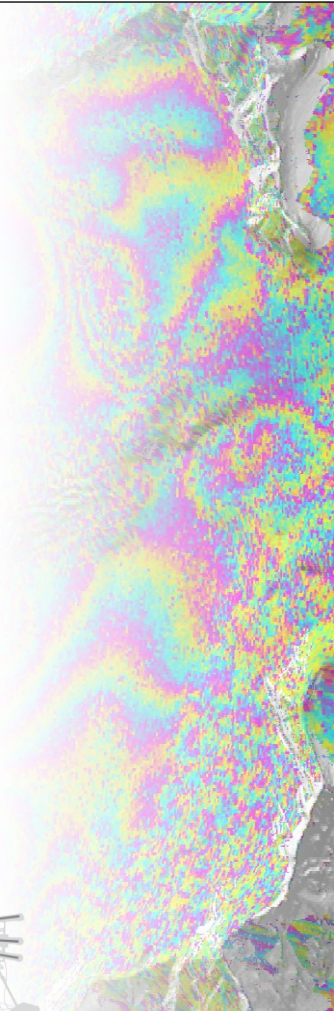
Public missions deliver **data free of charge** (esa missions), commercial data takes can cost **few thousand \$ each image**.

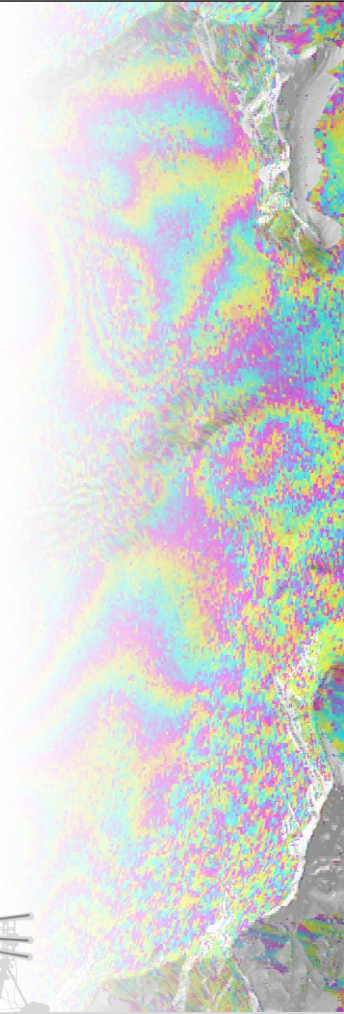
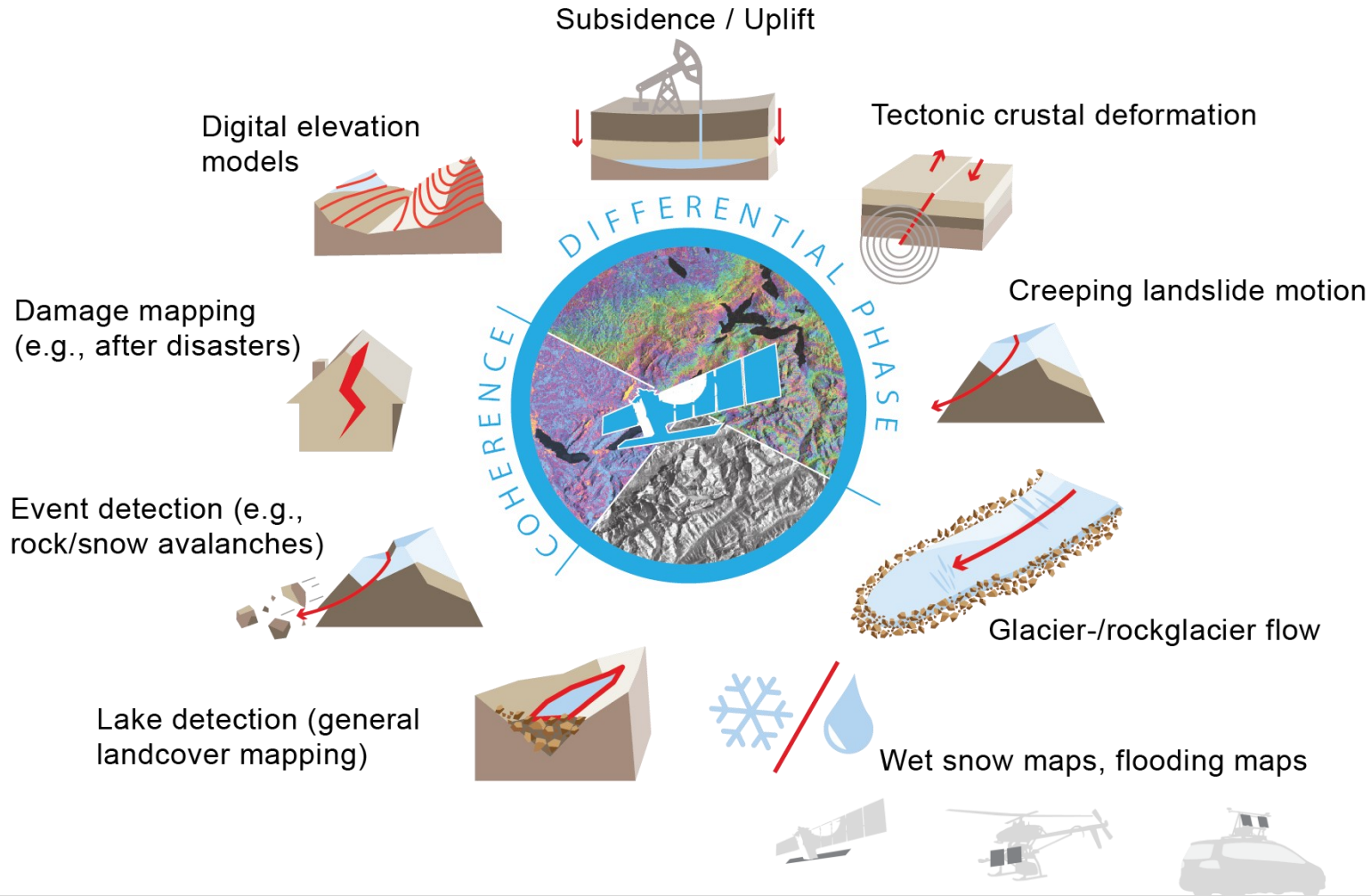


ERS-1 (Launch 1991) © esa



Sentinel-1 (Launch 2014) © esa

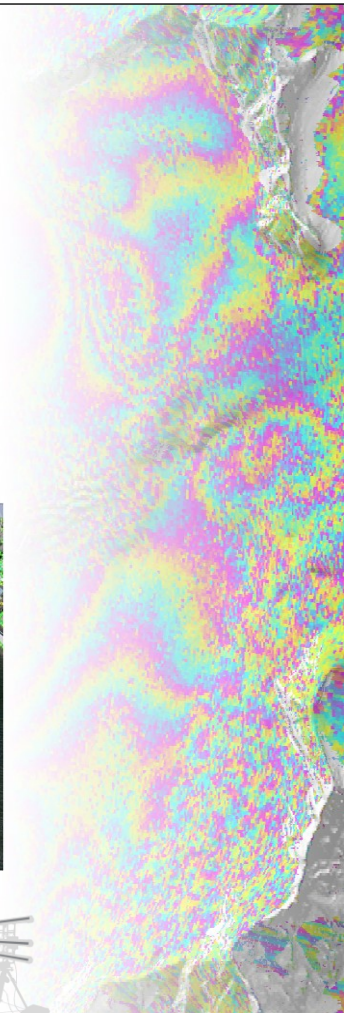
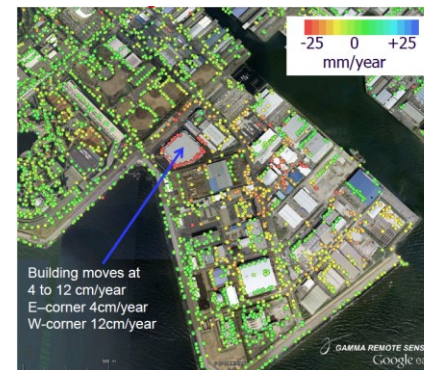


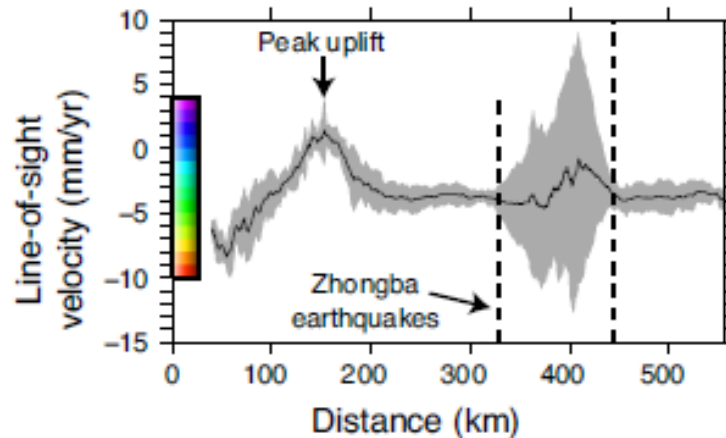
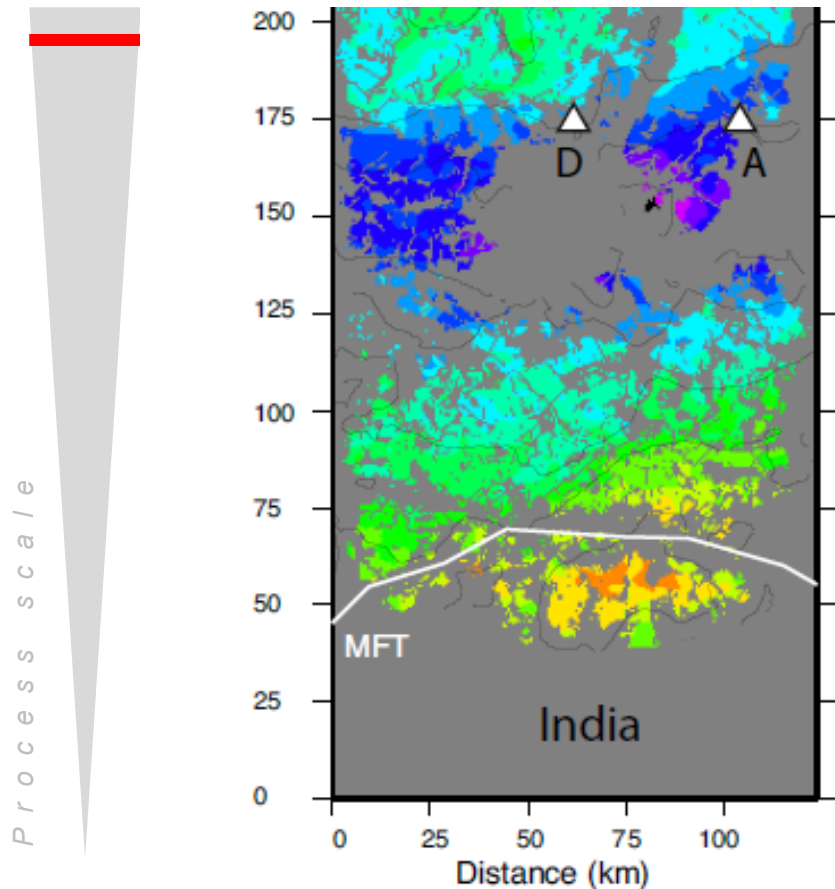


Process scale

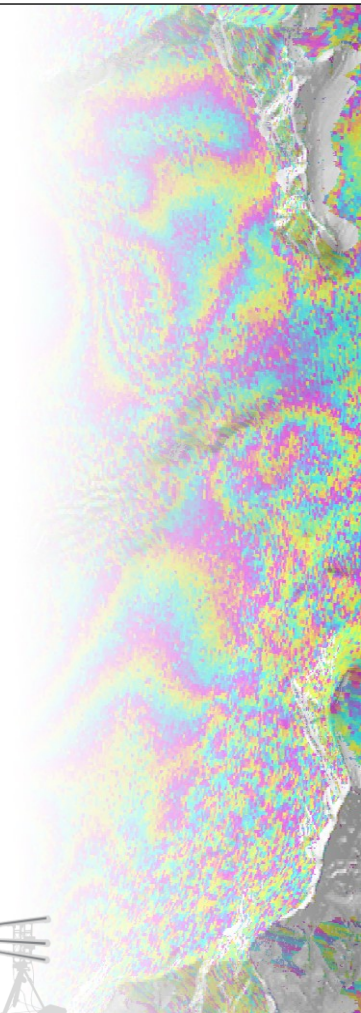
- Creeping tectonic motion (tectonic uplift)
- Crustal deformation (earthquakes)
- Large scale ground subsidence
- Glacier motion (e.g. with tracking)
- Landslide Motion
- Urban area deformation monitoring

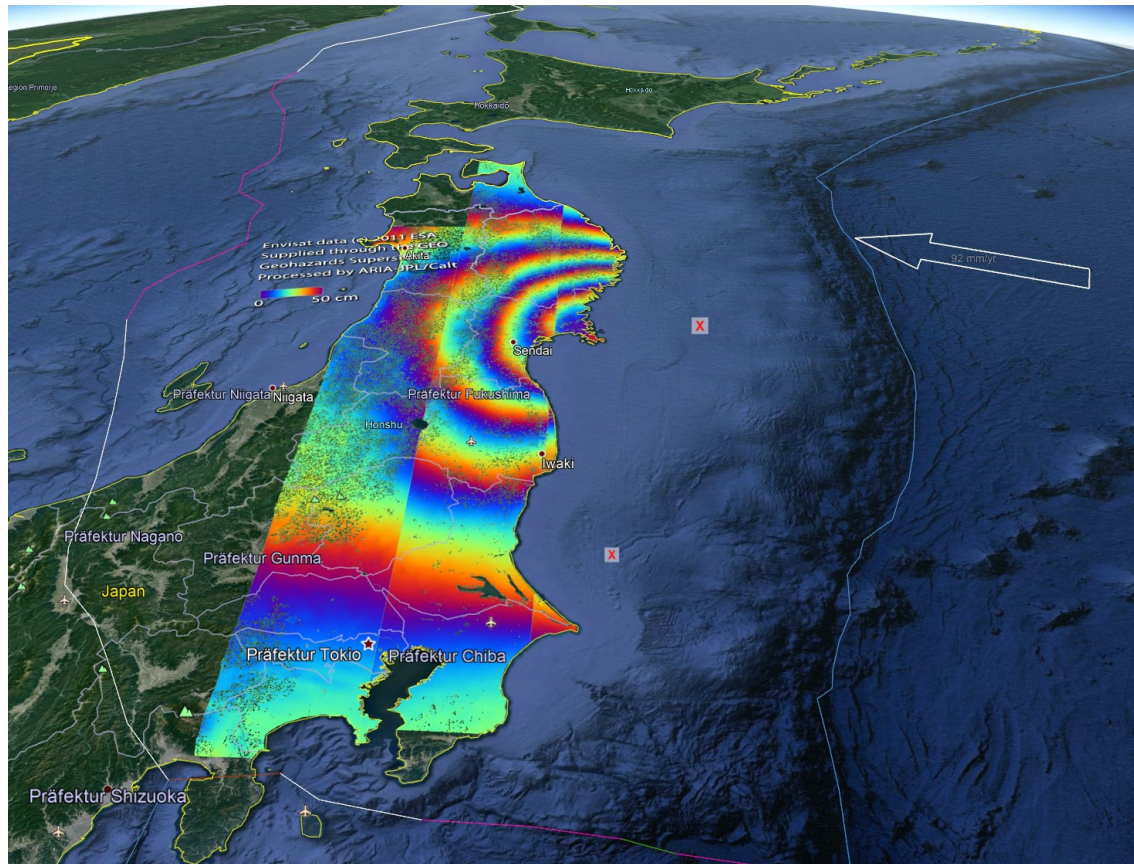
Ground Motion Service Germany





Grandin, R., Doin, M.-P., Bollinger, L., Pinel-Puysségur, B., Ducret, G., et al. Long-term growth of the Himalaya inferred from interseismic InSAR measurement. *Geology*, Geological Society of America, 2012, 40 (12), pp.1059 - 1062. 10.1130/G33154.1

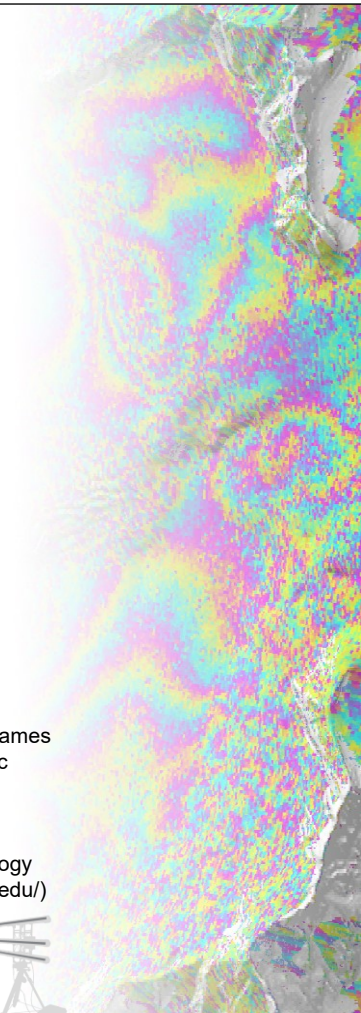


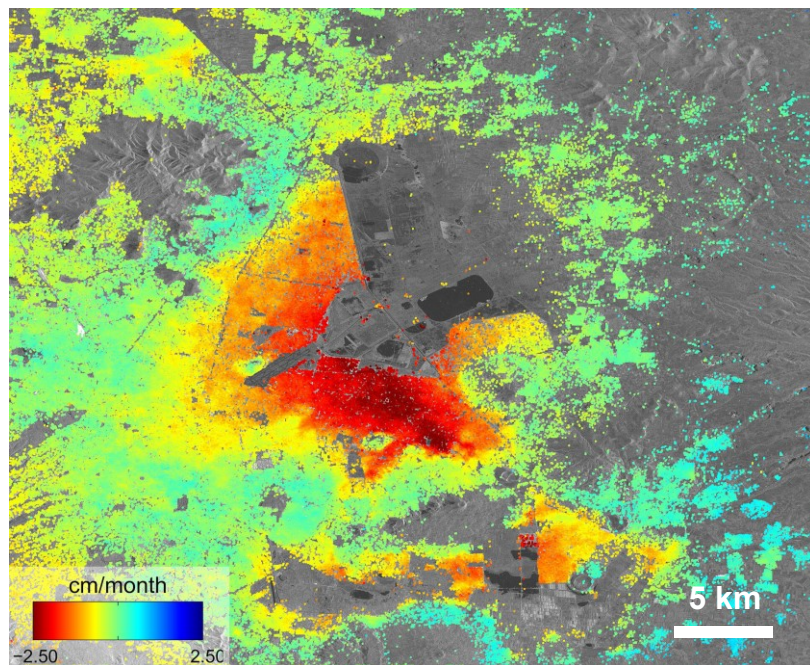


Process scale

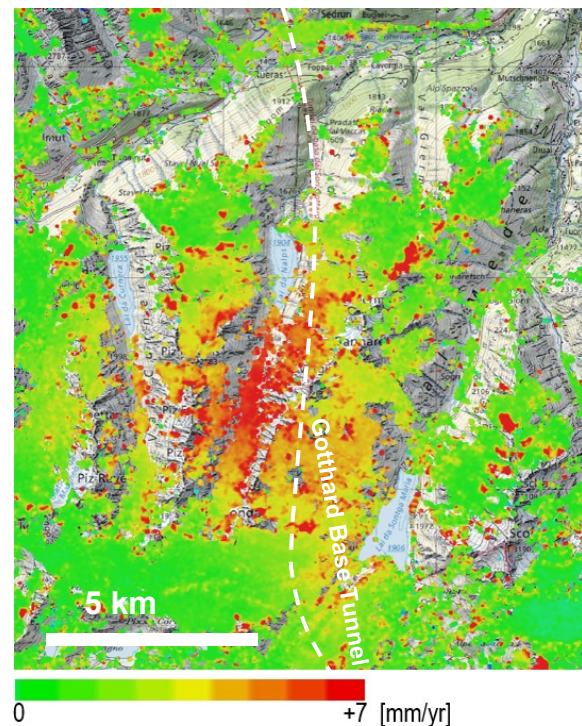
Mw 9.1 Tohoku-Oki Japan earthquake captured with 3 frames of ENVISAT ASAR co-seismic interferograms

© Tectonics Observatory :: California Institute of Technology (<http://www.tectonics.caltech.edu/>)

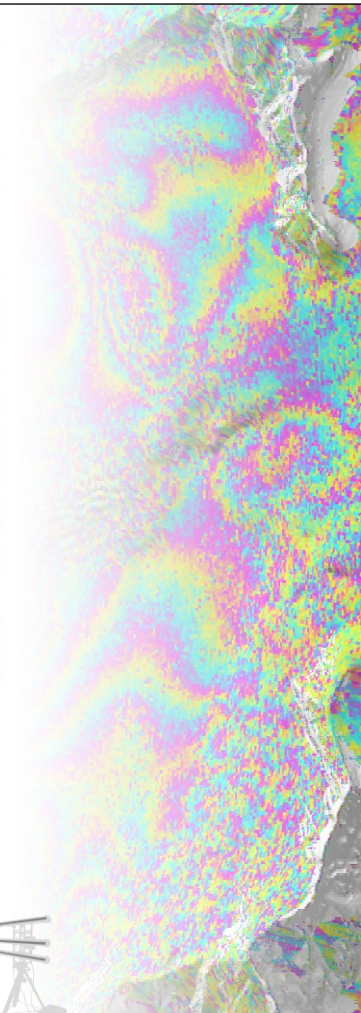




Mexico City ground subsidence measured using 5 Sentinel-1 scenes in 2014
 © Copernicus data (2014)/ESA/DLR Microwave and Radar Institute–SEOM InSARap study



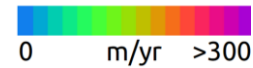
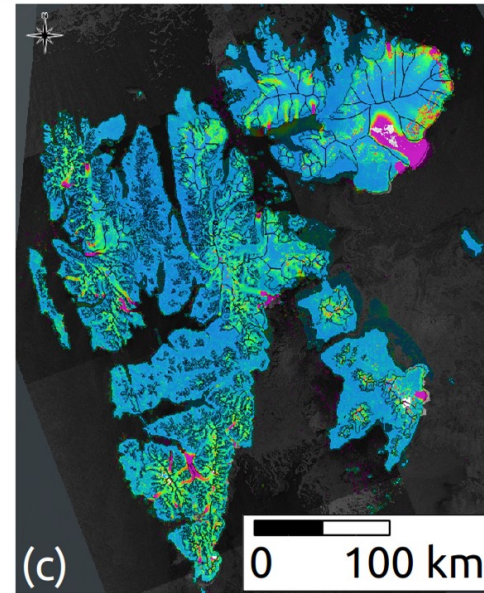
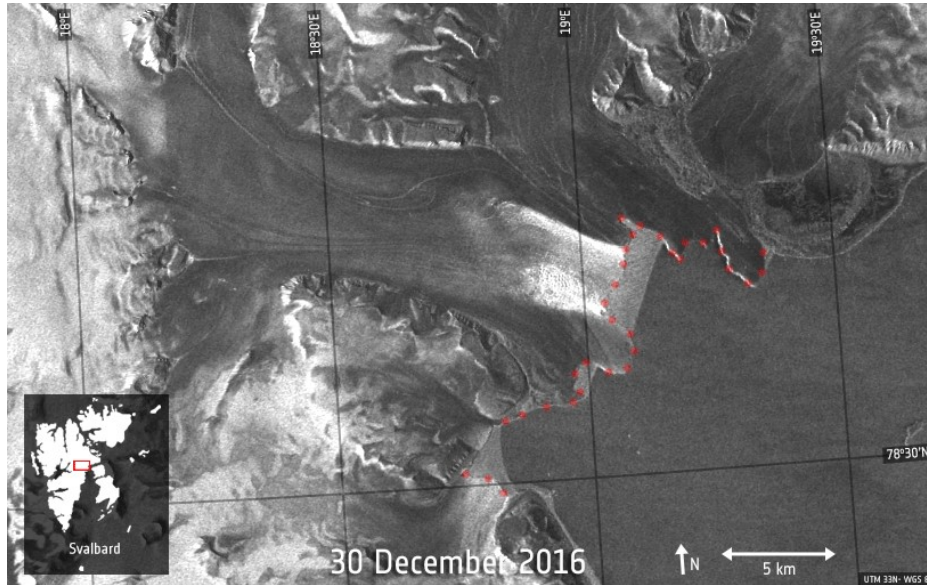
Val Nalps: Radarsat-2 data combined ascending & descending, only vertical direction. Data from 2011-2019.



Process scale

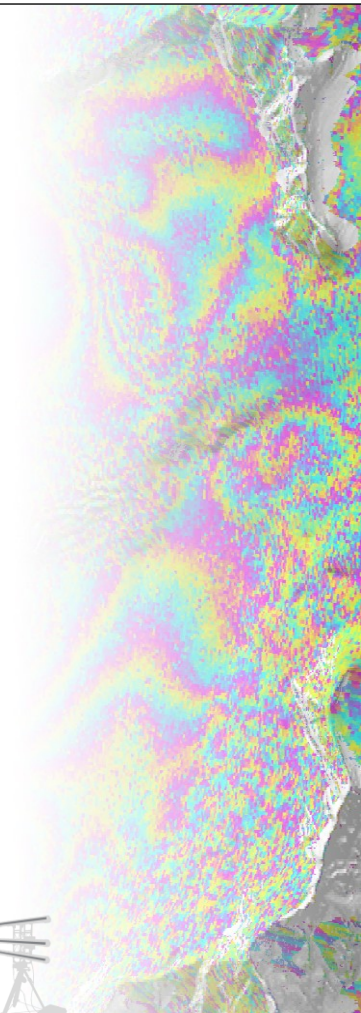


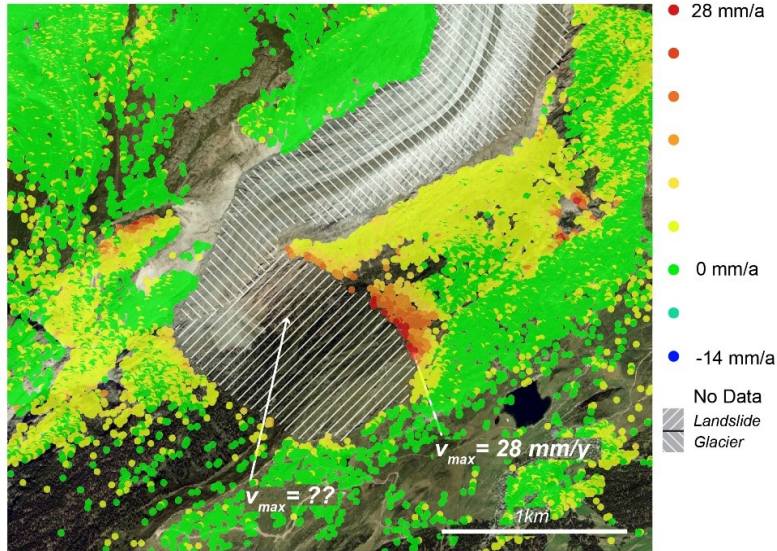
Process scale



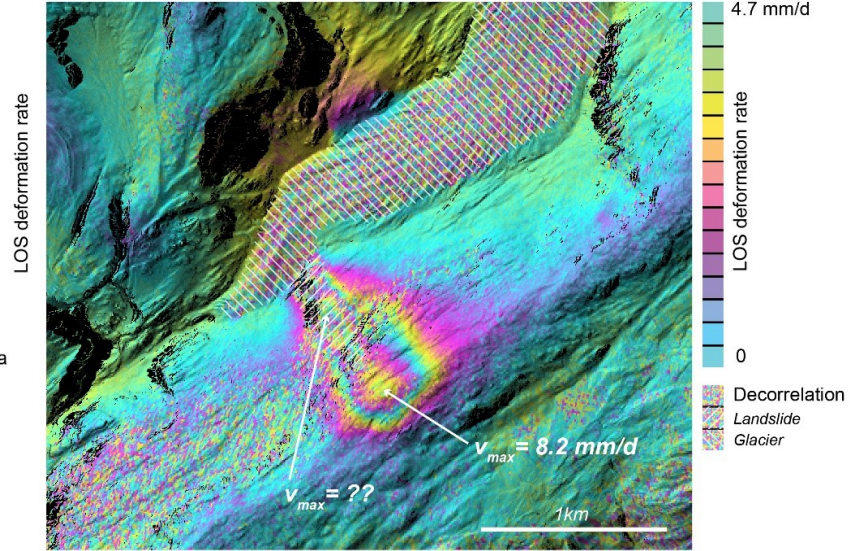
Radar images from the Copernicus Sentinel-1 mission show the sudden advance of the Negribreen glacier in Norway in early 2017 [image credit: ESA, the image contains modified Copernicus Sentinel-1 data (2016–17), processed by T. Strozzi (Gamma)]

Svalbard: Glacier velocity field derived from Copernicus Sentinel-1 data (2016-2017)

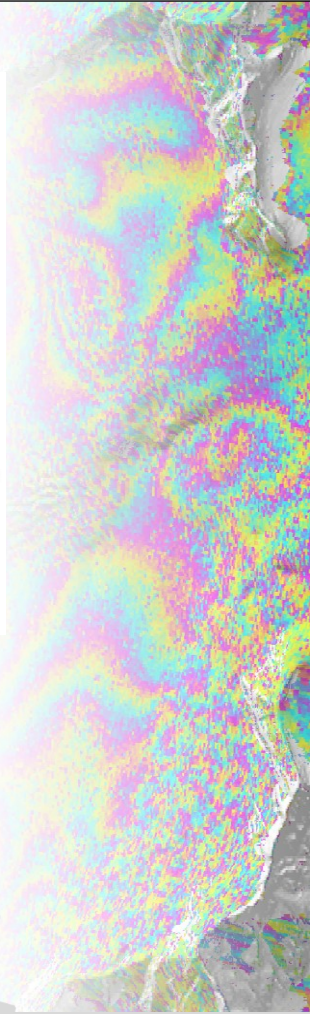


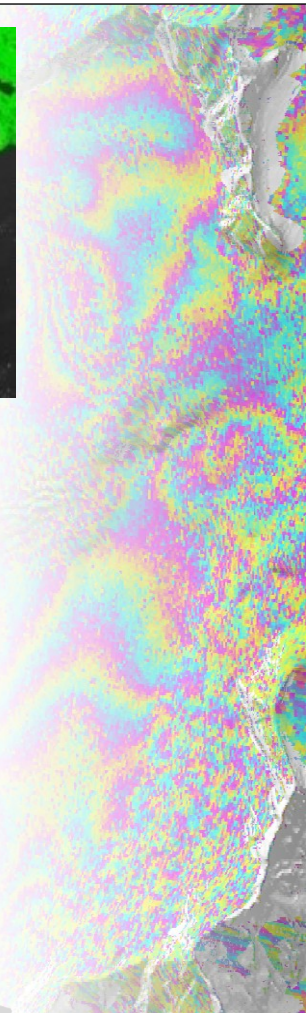
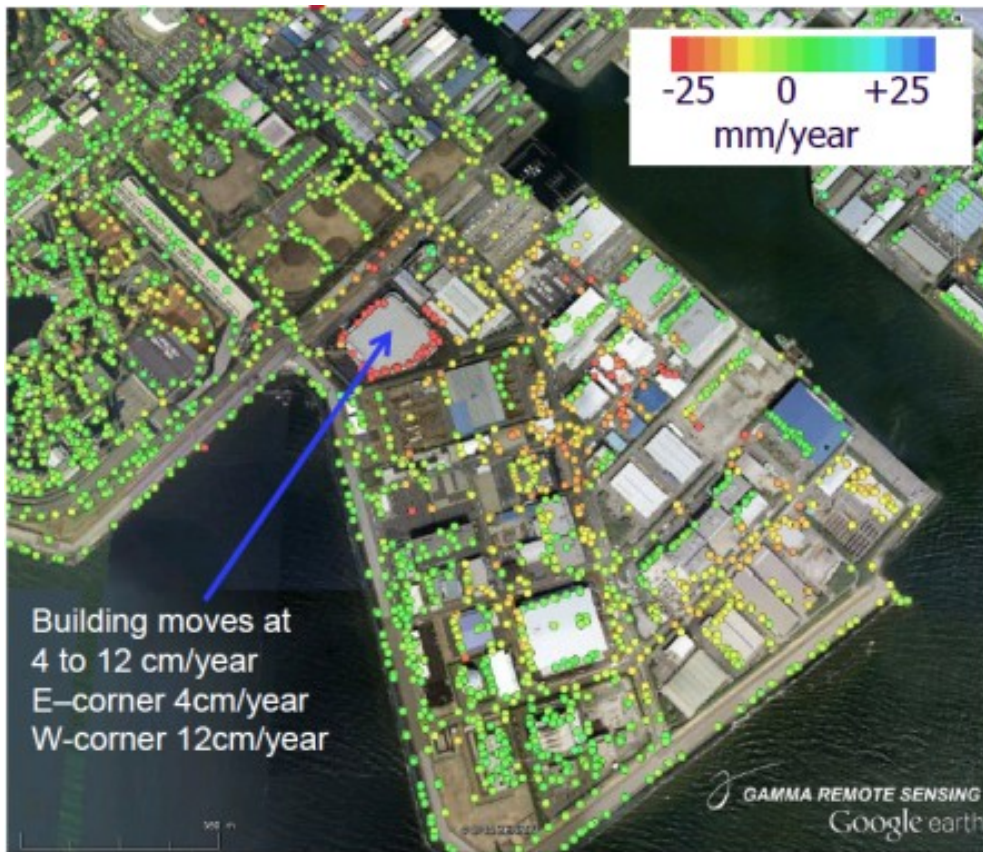


TerraSAR-X IPTA Displacement analysis of the Moosflue Area above the great Aletsch Glacier (Swiss Alps) for the year 2013. Precise measurements of slow to moderate movements are possible. Fast movements (Glacier and Main part of the Moosflue Landslide) cannot be measured with this method.



Sentinel-1 12-day interferogram covering the main movement of the Moosflue Landslide. The deformation field and the maximum displacement can be determined for the upper part. The fast movement of the lower part of the landslide leads to decorrelation and therefore missing information.





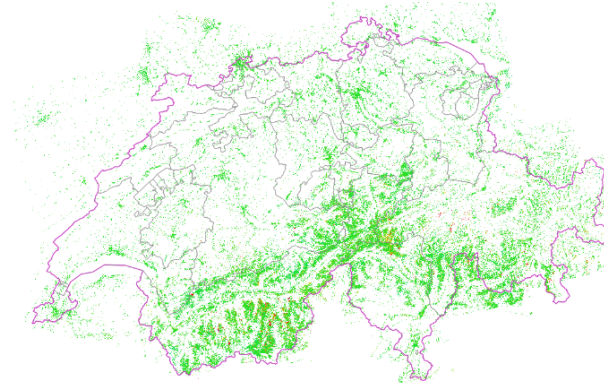
Funabashi, Japan, persistent scatterer interferometry using 28 ascending PALSAR (L-Band) Scenes.

Process scale



Satellite-InSAR boundary conditions

- No absolute measurements
- Only sensitive along line-of-sight
 - Intensity tracking (cross-and along-track detection possible)
- Side looking radar geometry (shadow and layover gaps in steep terrain)



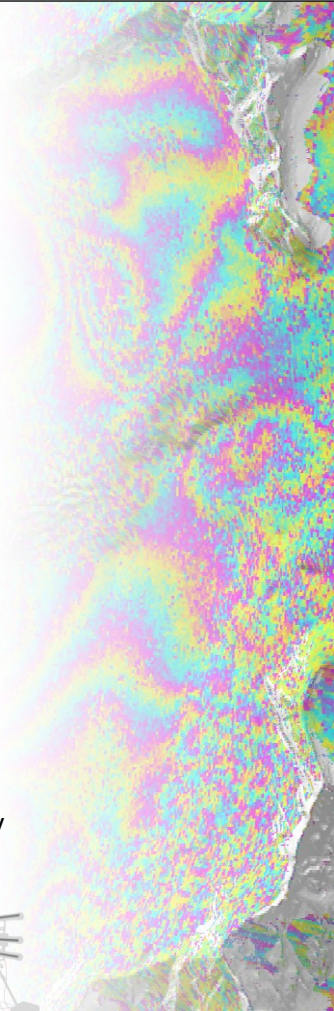
Compilation of PS-interferometry over Switzerland from ERS (1991-2000), ENVISAT ASAR (2004-2010), CSK, TSX und RSAT2 (2011-2019)

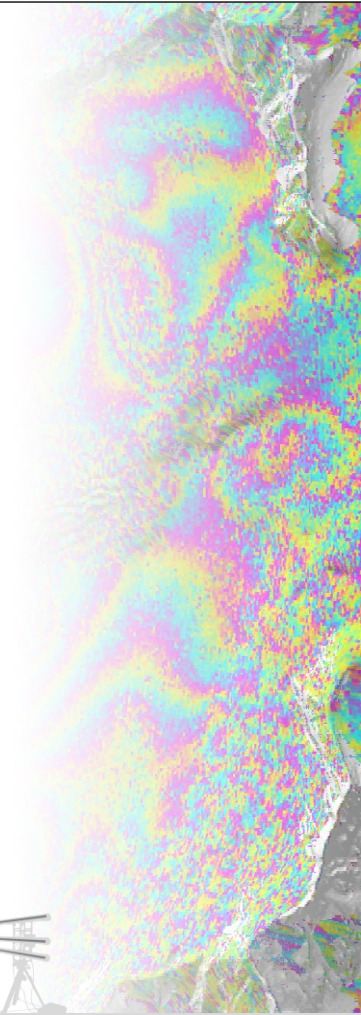
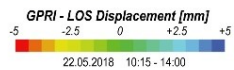
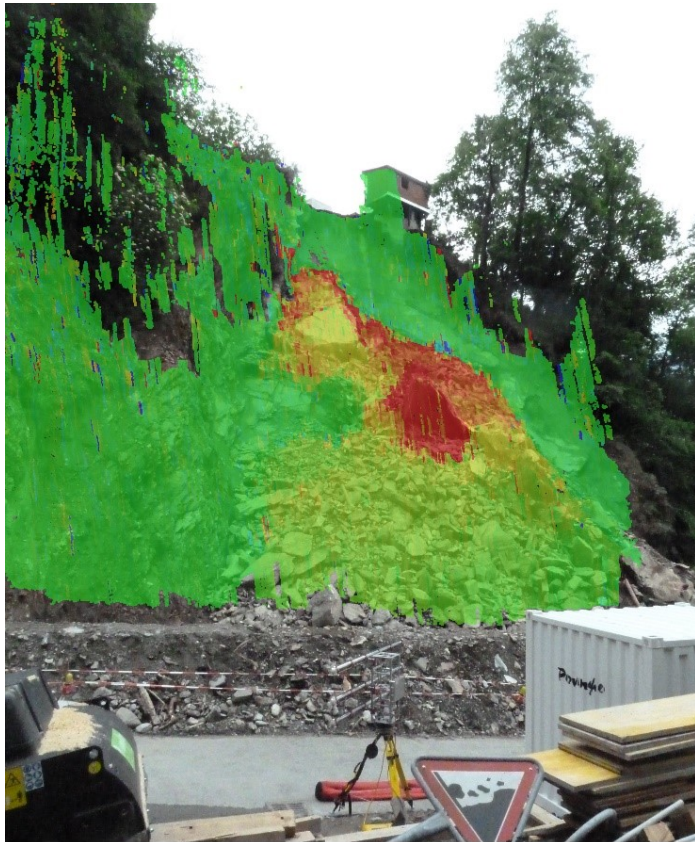


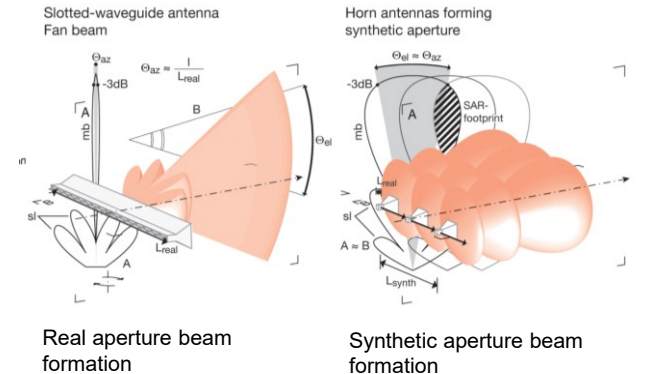
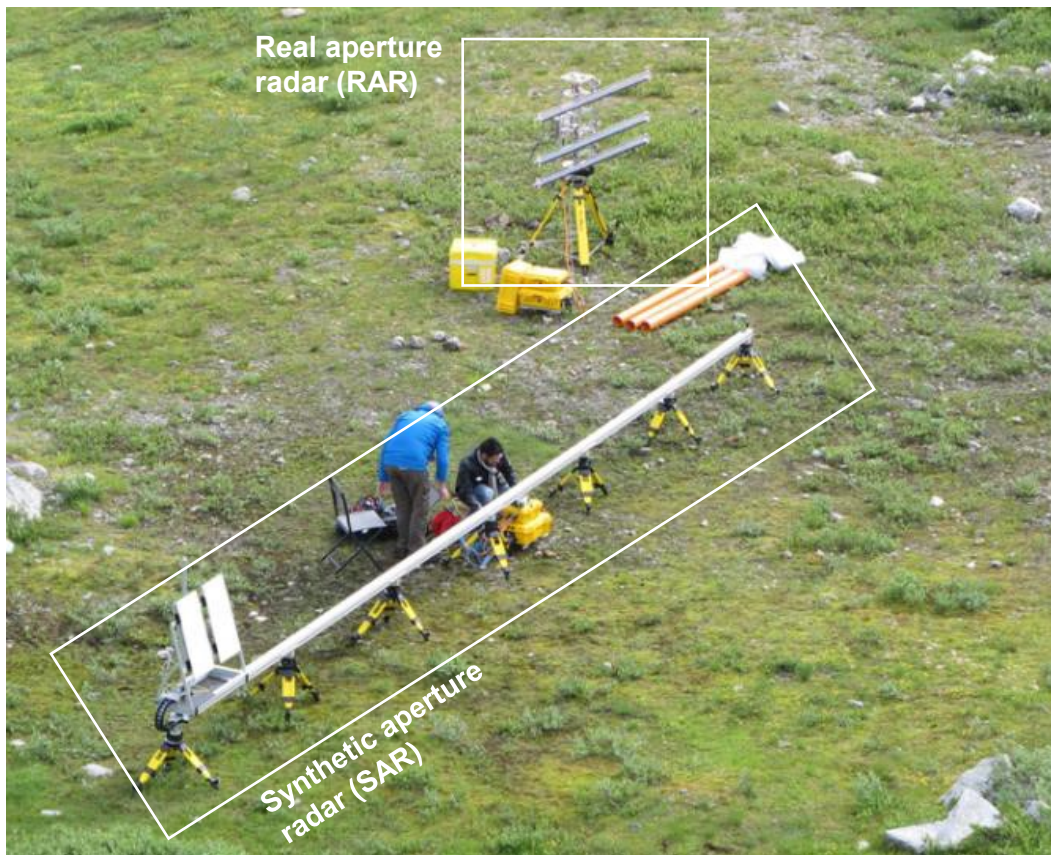
- Wide area mapping
- Marker-less mapping (no in-situ installation needed)
- In case for satellite-InSAR: Archive data!
- High precision and accuracy (mm-range for Satellite InSAR)
- Can be cost-effective (for large scale and using free satellite data)
- Increasing number of systems (commercial and open-data provider)



- Coherence needed (No information on vegetated areas)
- Measurement range is sensitive to unwrapping errors
- Can be expensive (for small scale and using commercial satellite data or very high resolution)
- Exact location of the scatterer in the footprint not precisely known (if no reflector is used)

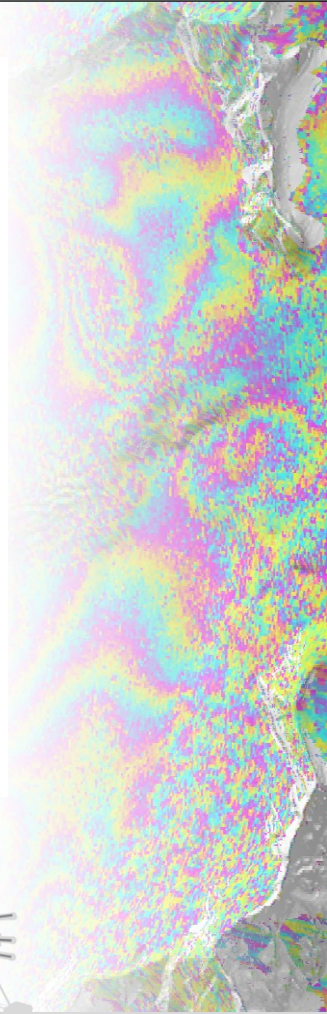
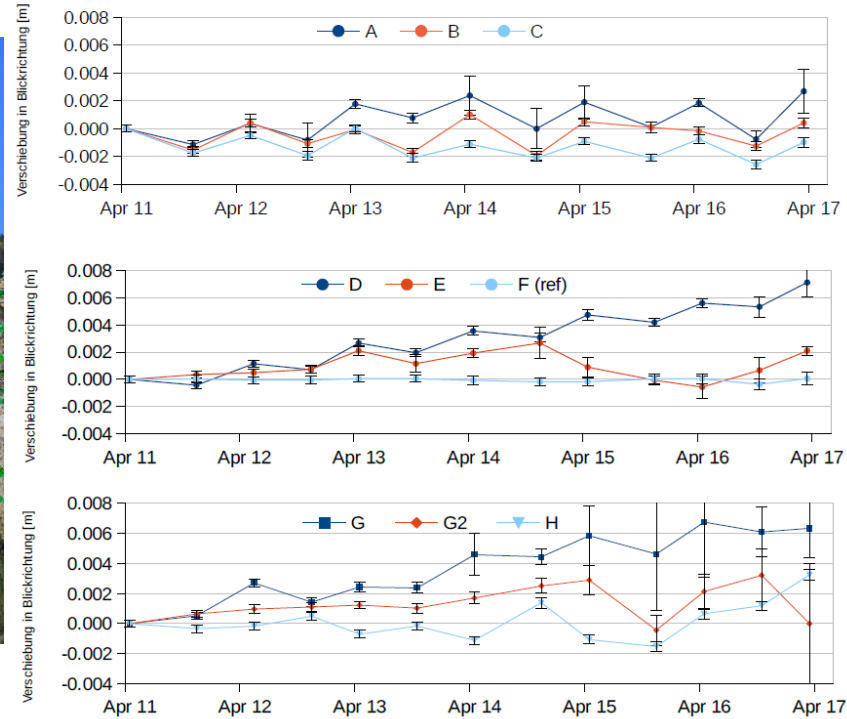
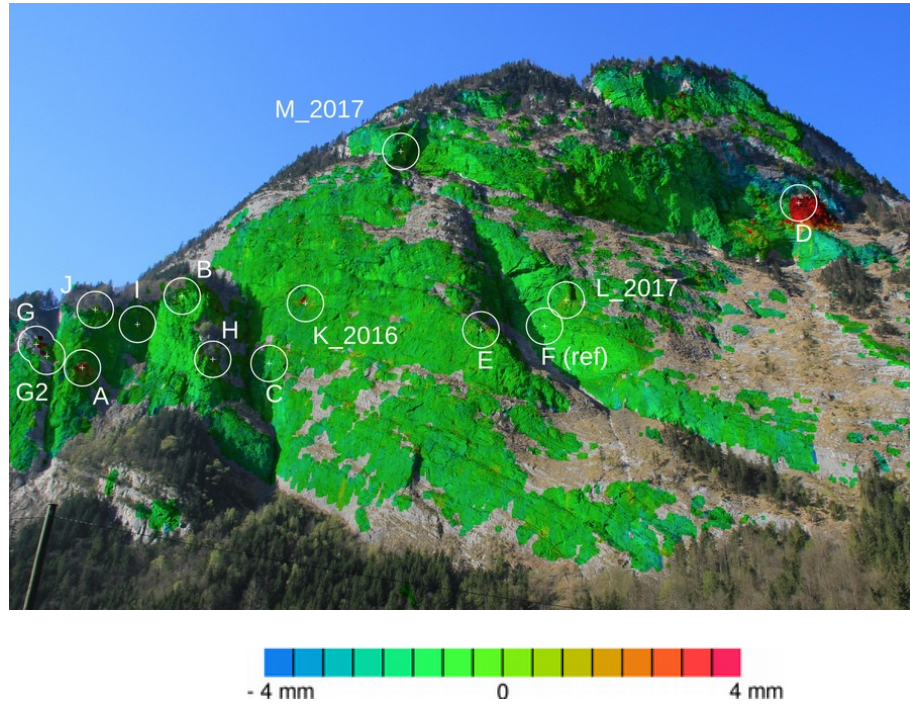


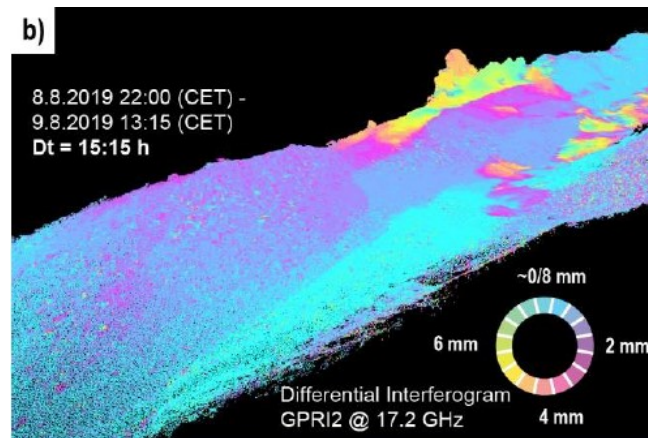




Caduff, R., Schlunegger, F., Kos, A., and Wiesmann, A. (2015) A review of terrestrial radar interferometry for measuring surface change in the geosciences, *Earth Surf. Process. Landforms*, 40, pages 208– 228, doi: [10.1002/esp.3656](https://doi.org/10.1002/esp.3656).

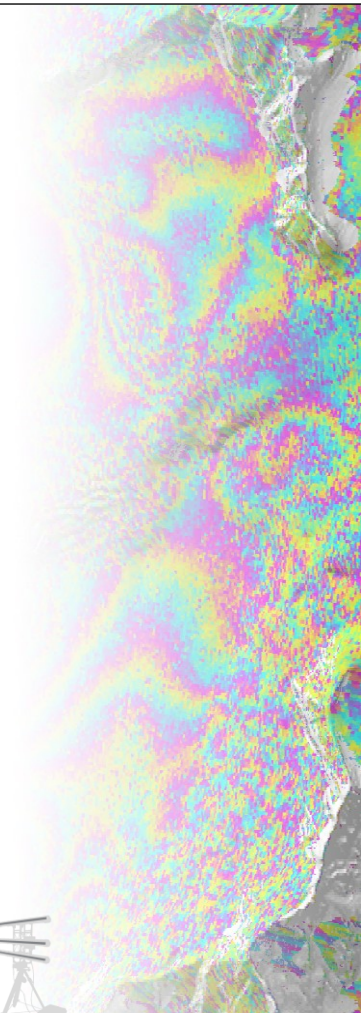


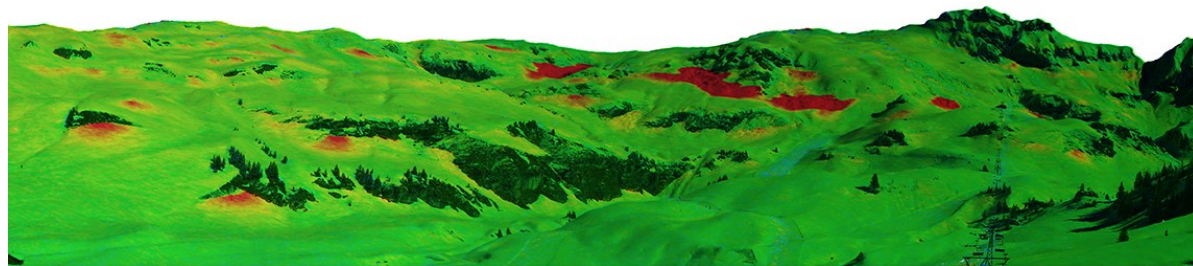
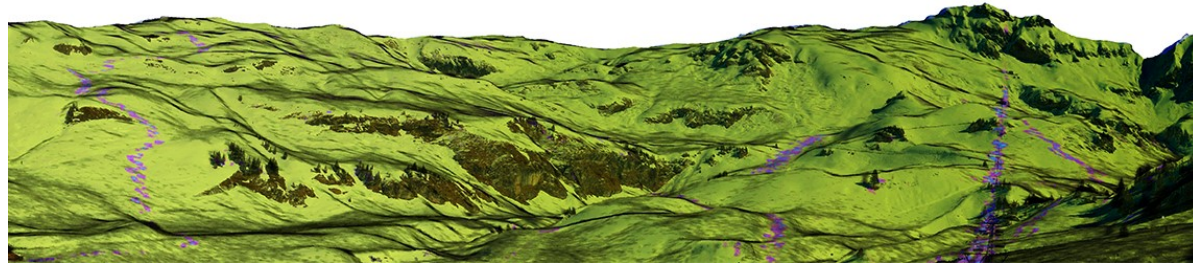




a) Setup of the terrestrial radar interferometer (GPRI) at location W. b) 15h Ku-Band interferogram from the west-flank in precise photo geometry. Different sectors with different kinematics could be delineated c) and identified as superficial movement (white) and most importantly as set of outcropping basal glide planes (red).

Caduff, R., Strozzi, T., Hählen, N., & Häberle, J. (2020, November). Accelerating Landslide Hazard at Kandersteg, Swiss Alps; Combining 28 Years of Satellite InSAR and Single Campaign Terrestrial Radar Data. In *Workshop on World Landslide Forum* (pp. 267-273). Springer, Cham.



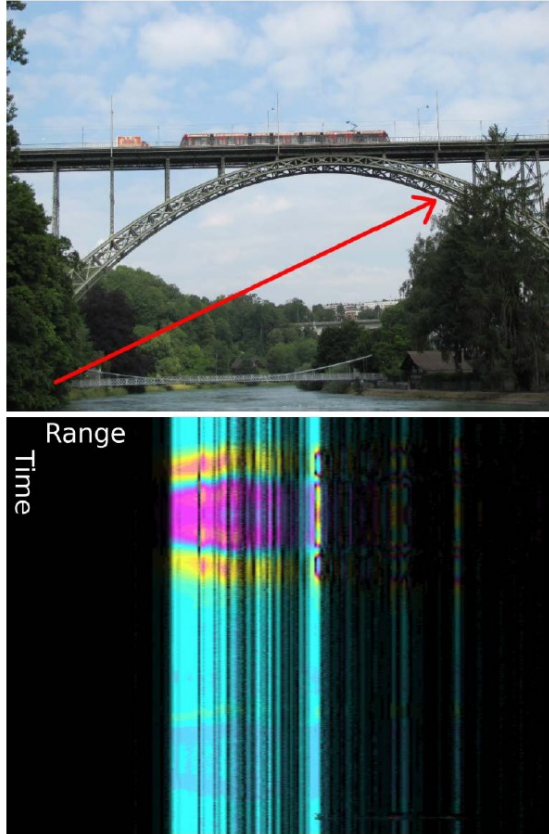


0  12 LOS displacement [cm/day]

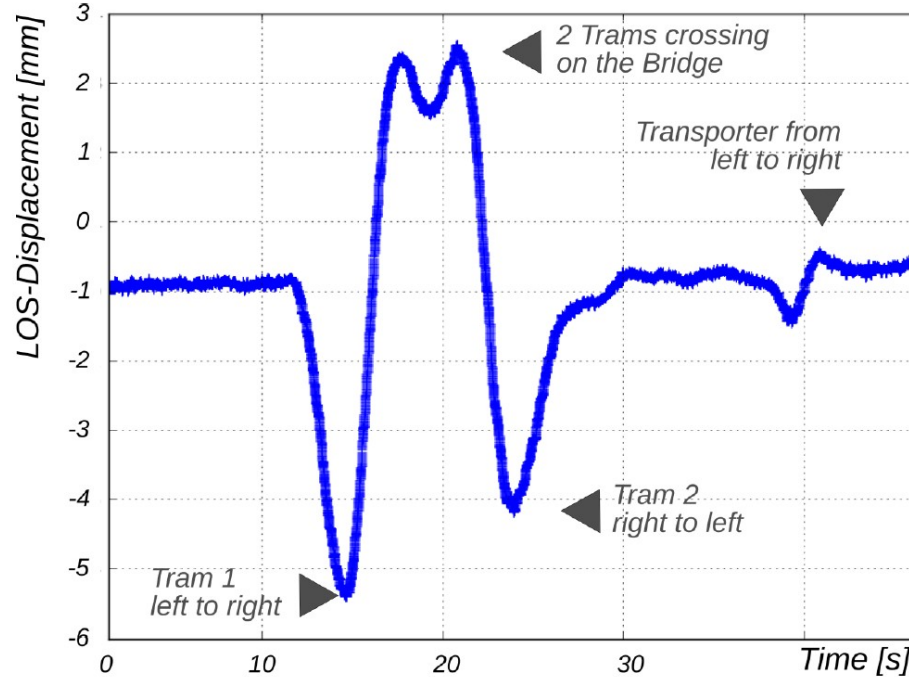


Caduff, R., Wiesmann, A., Bühler, Y. and Pielmeier, C. (2015), Continuous monitoring of snowpack displacement at high spatial and temporal resolution with terrestrial radar interferometry. *Geophys. Res. Lett.*, 42: 813– 820. doi: [10.1002/2014GL062442](https://doi.org/10.1002/2014GL062442).



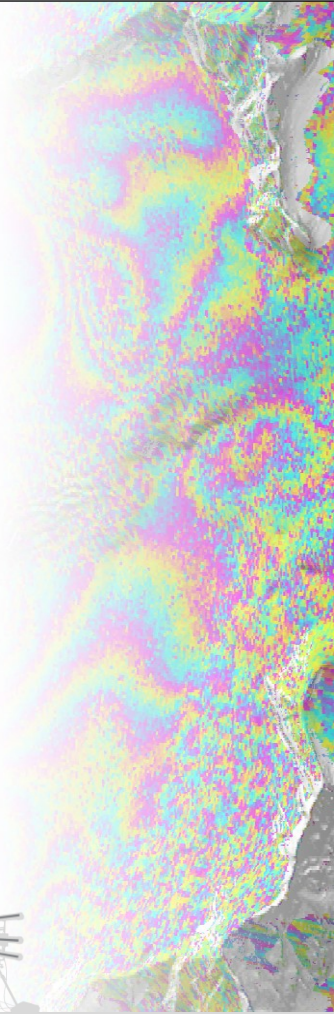


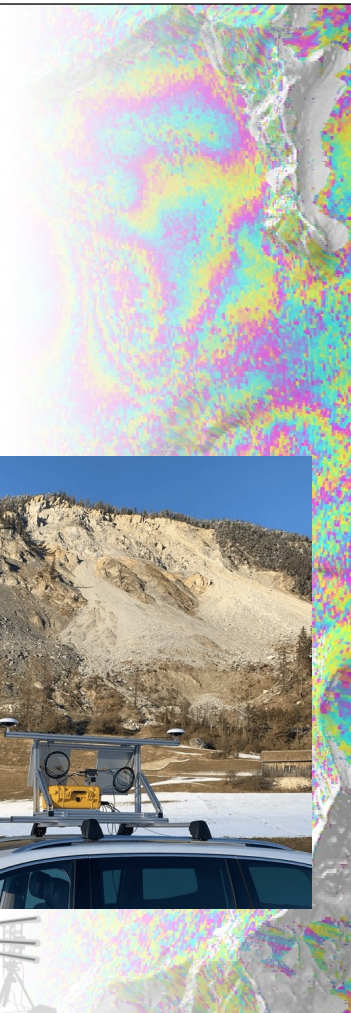
Deformation measurements of the Kornhaus-Bridge (Bern) during traffic with the fixed look mode



Werner et al. (2012)

Werner, C., Wiesmann, A., Strozzi, T., Kos, A., Caduff, R., & Wegmüller, U. (2012, April). The GPRI multi-mode differential interferometric radar for ground-based observations. In EUSAR 2012; 9th European Conference on Synthetic Aperture Radar (pp. 304-307). VDE.



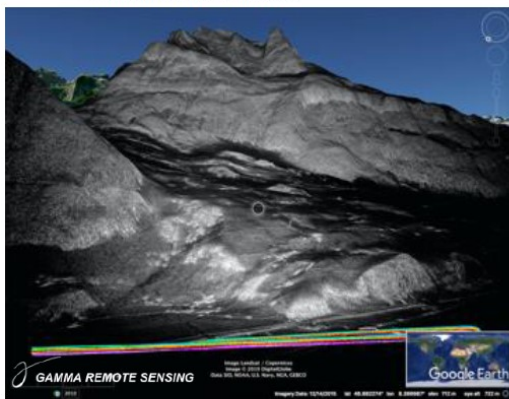


Frey, O., Werner, C. L., Manconi, A. and Coscione, R. "Measuring surface displacements using a novel UAV/car-borne radar interferometer: including a case study on a fast-moving landslide in Brinzauls." Abstract Volume 18th Swiss Geoscience Meeting. Berne, Zurich: (SCNAT); ETH Zurich, 2020. pp. 502-502.

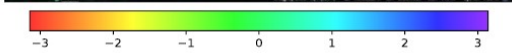
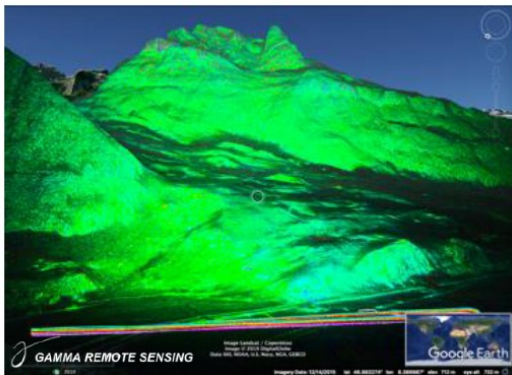




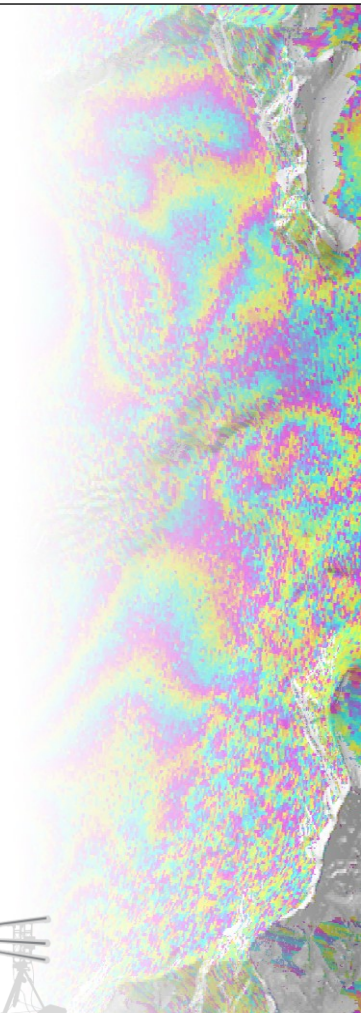
Area of interest on the campaign day. On the lower right, the local GNSS reference station is situated to obtain a highly precise post-processed kinematic GNSS solution of the UAV position.

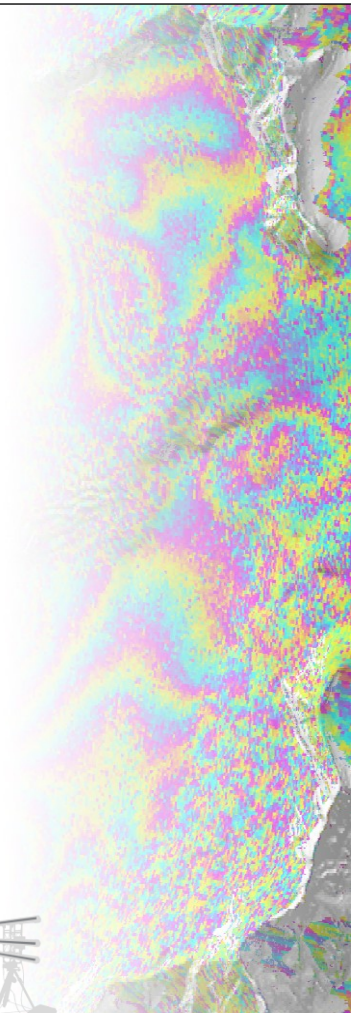


Google Earth (GE) view of UAV-borne L-band SAR backscatter intensity image with UAV flight trajectories in the foreground.



Google Earth view of UAV-borne L-band differential interferometric phase (left) and coherence (right) for nominally zero spatial baseline and a temporal baseline of 3 minutes. The flight tube of these two repeat-tracks are within 1m radius. With the exception of forested areas in the near range and areas with severe foreshortening a very high coherence is obtained and the interferometric phase is also stable.





GAMMA Remote Sensing AG, Switzerland
Worbstrasse 225
CH-3073 Gümligen
+41 31 951 70 05
www.gamma-rs.ch

Rafael Caduff
caduff@gamma-rs.ch

